CHEMISTRY OF MATERIALS

ARTICLE

pubs.acs.org/cm

Oxygen-Deficient Perovskite $Sr_{0.7}Y_{0.3}CoO_{2.65-\delta}$ as a Cathode for Intermediate-Temperature Solid Oxide Fuel Cells

Yan Li,[†,‡] Young N. Kim,[†] Jinguang Cheng,[†] José A. Alonso,[§] Zhiwei Hu,[∥] Yi-Ying Chin,[∥] Tsuyoshi Takami,[⊥] Maria T. Fernández-Díaz,[#] Hong-Ji Lin,[▽] Chien-Te Chen,[▽] Liu H. Tjeng,[∥] Arumugam Manthiram,[†] and John B. Goodenough[†,*]

[†] Materials Science and Engineering Program and Department of Mechanical Engineering, University of Texas at Austin, Texas 78712, United States

[‡] College of Physical Science and Technology, Heilongjiang University, Harbin 150080, China

[§] Instituto de Ciencia de Materiales de Madrid, CSIC, Cantoblanco, E-28049 Madrid, Spain

[∥] Max Planck Institute for Chemical Physics of Solids, Nöthnitzerstr, 40, D-01187 Dresden, Germany

[⊥] Department of Physics, Graduate School of Science, Osaka University, 1-1 Machikaneyama-cho, Toyonaka, Osaka 560-0043, Japan

[#] Institut Laue Langevin, BP 156X, Grenoble, F-38042, France

[▽] National Synchrotron Radiation Research Center, HsinChu 30077, Taiwan

ABSTRACT: The oxygen-deficient perovskite $Sr_{0.7}Y_{0.3}CoO_{2.65-\delta}$ contains $Co2O_{6/2}$ (001) planes alternating with oxygen-deficient $Co1O_{1.15-\delta}$ planes having $0.15-\delta$ O4 oxygen in the plane capping tetrahedral site Co1. With ordering of the O4 atoms below 300 °C, the oxide exhibits n-type polaronic conduction associated with localized high-spin 3d electronic configurations on Co^{2+} in Co1 sites; a transition to itinerant-hole conduction occurs on disordering of O4 ions over the range $350 < T < 600$ °C. Above 600 °C, $Sr_{0.7}Y_{0.3}CoO_{2.65-\delta}$ is a mixed oxide-ion/electronic conductor exhibiting good activity for the oxygen-reduction reaction, which makes it a competitive cathode material for an intermediate-temperature solid oxide fuel cell.

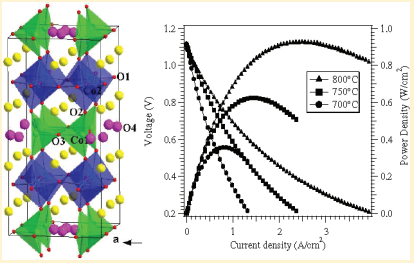

KEYWORDS: solid oxide fuel cell, oxygen-reduction reaction, oxygen-deficient perovskite, polaronic to itinerant electronic transition

1. INTRODUCTION

The solid oxide fuel cell (SOFC) converts the chemical energy of the reaction of a fuel with oxygen directly into electrical energy. The rate-limiting step of this electrochemical conversion is the oxygen-reduction reaction (ORR) at the cathode. While operating above 500 °C, the cathode of the SOFC has no bound water on the surface of the cathode where O_2 adsorption and reduction occurs. A cathode active for the ORR must be a good electronic conductor, but delivery of the electrons from the anode to the adsorbed O_2 on the cathode may occur either near a triple-phase boundary between air/cathode/O^{2-}-ion electrolyte or over a broader surface area of a mixed O^{2-}-ion/electron conductor (MIEC) in contact with the O^{2-}-ion solid electrolyte. The perovskite $La_{1-x}Sr_xMnO_3$ cathode operates in the former mode; the latter mode is found with the Co-containing oxygen-deficient perovskites $Ln_{1-x}Sr_xCo_{1-y}Fe_yO_{3-\delta}$ (Ln = rare earth),[1] $Ba_{1-x}Sr_xCo_{1-y}Fe_yO_{3-\delta}$,[2,3] and $LnBaCo_2O_{5+\delta}$.[4,5] Here, we report the electronic transport and the activity for the ORR of the oxygen-deficient cobalt perovskite $Sr_{0.7}Y_{0.3}CoO_{3-\delta}$.

$Sr_{0.7}Y_{0.3}CoO_{2.63}$ (SYCO) has recently been reported to crystallize with a novel ordering of the oxygen vacancies that gives a tetragonal structure, space group $I4/mmm$, with unit-cell parameters $a \approx 2a_p$, $c \approx 4a_p$, where a_p is the parameter of the cubic perovskite unit cell.[6] As is illustrated in Figure 1, the oxygen vacancies of SYCO are ordered into alternate $Co1O_{1.15-\delta}$ (001) planes of the perovskite structure, as occurs in the brownmillerite structure of $CaFeO_{2.5}$; the $Co2O_3$ planes contain corner-shared $Co2O_{6/2}$ octahedra, as in the perovskite structure. In SYCO, the additional 0.13 O4 per formula unit enter the $Co1O_{1.15-\delta}$ planes to create five-coordinated Co1 in addition to the four-coordinated Co1 of the brownmillerite structure. A Co1−O4 bond length of 2.156(7) Å is significantly longer than that of Co1−O2, 1.850(3) Å, and of Co1−O3, 1.928(1) Å, signaling a relatively weak Co1−O4 bond[6] and a mobile $(O4)^{2-}$ ion. However, a combined electron-diffraction and synchrotron XRD study[7] at room temperature has indicated an oxygen vacancy ordering within the $Co1O_{1.15-\delta}$ layers associated with the ordering of the Sr^{2+} and Y^{3+} ions, and a high-temperature synchrotron XRD study[8] has shown that the oxygen vacancies undergo an order−disorder transition at $T_s \approx 550$ K in $Sr_{0.67}Y_{0.33}CoO_{3-\delta}$. Therefore, we can anticipate a high O^{2-}-ion mobility above 600 °C within the $Co1O_{1.15-\delta}$ planes, which would be adequate for the cathode of an intermediate-temperature (IT) SOFC. Thermogravimetric analysis (TGA) of SYCO samples appears to confirm

Received: August 25, 2011
Revised: September 29, 2011
Published: October 24, 2011

dx.doi.org/10.1021/cm202542q | *Chem. Mater.* 2011, 23, 5037–5044

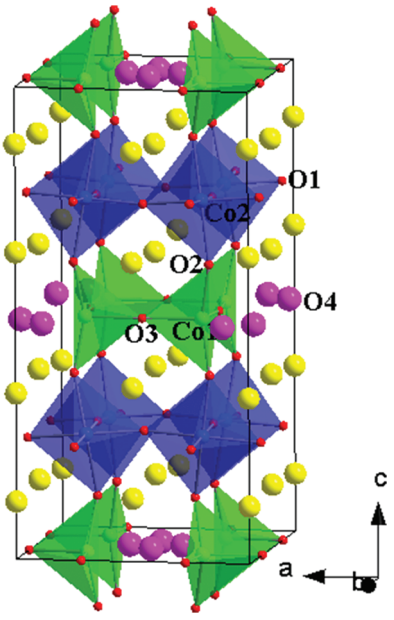

Figure 1. Crystal structure of the oxygen-deficient perovskite $Sr_{0.7}Y_{0.3}CoO_{2.65-\delta}$. Note that only about $^1/_4$ of the O4 atoms are occupied.

this conjecture,[6] but the electrochemical performance of SYCO as the cathode of an IT-SOFC has not been reported, and little is known about the electronic transport properties of SYCO above room temperature.

To investigate SYCO as a potential cathode for an IT-SOFC, we have prepared polycrystalline SYCO by solid-state reaction and characterized its crystal structure, oxygen evolution, valence and spin states of the Co ions, and electronic transport properties with X-ray and neutron powder diffraction, TGA, X-ray absorption spectroscopy, and electrical conductivity and thermopower measurements over a wide temperature range. The polarization resistance and electrochemical performance of a SYCO cathode supported on a $La_{0.8}Sr_{0.2}Ga_{0.83}Mg_{0.17}O_{2.815}$ (LSGM) electrolyte were then tested in the intermediate temperature range 700−800 °C. A maximum power density of 927 mW/cm^2 at 800 °C demonstrated that SYCO is a promising cathode material for IT-SOFCs.

2. EXPERIMENTAL SECTION

2.1. Synthesis. Polycrystalline SYCO samples were prepared by solid-state reaction according to ref 6. Stoichiometric mixtures of analytical grade $SrCO_3$, Y_2O_3, and Co_3O_4 powders were thoroughly mixed in an agate mortar, pressed into pellets, and then sintered in air at 1000−1100 °C for 4 days with several intermediate grindings. During the last sintering, the furnace was switched off and the sample was allowed to cool gradually in the furnace; we denoted this sample hereafter as "furnace-cooled". As was done in a previous paper,[9] a quenched sample was also obtained by plunging the sample from 1100 °C into liquid N_2. As determined by iodometric titration,[9] the oxygen concentration of the furnace-cooled sample was similar to that of the quenched one, that is, $O_{2.63}$ vs $O_{2.62}$. However, rather than the ordered arrangement of the oxygen vacancies in the furnace-cooled sample, the oxygen vacancies should remain disordered at room temperature in the quenched sample.

2.2. Structural and Thermal Characterizations. The obtained products were first characterized by powder X-ray diffraction (XRD) for phase identification and to assess phase purity with a Philips X'pert diffractometer (Cu Kα radiation, λ = 1.5418 Å) in Bragg−Brentano reflection geometry. Room-temperature neutron powder diffraction (NPD) data were then collected in the diffractometer D2B at the Institut Laue-Langevin, Grenoble, with a neutron wavelength λ = 1.594 Å within the 2θ range from 9 to 157°. About 2 g of sample was used for the NPD. The obtained NPD profile was analyzed by the Rietveld method with the FullProf program and the use of its internal tables for scattering lengths. The line shape of the diffraction peaks was generated by a pseudo-Voigt function. In the final run, the following parameters were refined: background points, zero shift, half-width, pseudo-Voigt, and asymmetry parameters for the peak shape, scale factor, unit-cell parameters, positional and occupancy factors, and isotropic thermal factors. High-temperature NPD data were collected at the HRPT high-resolution diffractometer (λ = 1.494 Å) in the Paul Scherrer Institut (PSI, Switzerland). About 3 g of sample were loaded into a steel tube open at ambient atmosphere and placed in the isothermal zone of a furnace with a vanadium resistor operating under vacuum ($P_{O2} \approx 10^{-6}$ Torr). Several patterns were collected at 373, 473, 573, 673, 873, and 1073 K; the counting time was typically 3 h per pattern.

The initial oxygen content of the obtained SYCO samples was chemically determined by iodometric titration. The evolution of the oxygen concentration during thermal cycling in air was determined by TGA with a Perkin-Elmer TGA 7 thermal analysis system in the temperature range 30−900 °C with a heating/cooling rate of 2 °C/min. About 50 mg of the SYCO sample was used in the TGA experiment.

2.3. X-ray Absorption Spectroscopy (XAS). XAS spectra at the Co−$L_{2,3}$ and O−K edges were measured at the BL11A beamline of National Synchrotron Radiation Research Center (NSRRC) in Taiwan. The Co−$L_{2,3}$ spectra were taken in the total electron yield (TEY) mode and the O−K in the fluorescence yield (FY) mode with a photon energy resolution of 0.3 and 0.2 eV, respectively. The pellet samples were cleaved *in situ* in an ultrahigh-vacuum chamber with pressure in the 10^{-10} mbar range. NiO and CoO single crystals were also measured *simultaneously* to serve as the energy reference for the O−K and Co−$L_{2,3}$ edges, respectively.

2.4. Electrical Conductivity and Thermopower Measurements. The electrical conductivity was measured with a standard dc four-probe method in the temperature interval 100−1073 K. The low-temperature (T < 300 K) measurements were performed on a specimen with a rectangular geometry, having typical size of 0.5 × 0.5 × 3 mm^3, within a closed-circle refrigerator with He gas as the refrigerant. Four pieces of copper wire were attached to the surface of the specimen via an Indium pad. To eliminate the contribution of the contact and thermoelectric potentials, the voltage was recorded with ± current at each sampling point. The electrical conductivity above room temperature was performed in air on a cylindrical rod 6.5 mm in diameter and ∼10 mm in length. Pt wire and Pt paste were used to make the four probes. At each temperature point, an I−V scan from −100 mA to 100 mA with a step of 10 mA was performed, and the electrical conductivity was calculated from the slope of the obtained straight line.

The thermopower was measured with a two-probe method in a homemade apparatus in the temperature interval 100−773 K in air. The specimen was mounted between two heater stages, each controlled independently by a temperature controller. In a typical run, a constant temperature gradient ΔT = 4 K was used over the entire temperature range. After making a correction for the copper−lead contribution, the thermopower of the specimen becomes $\alpha = \alpha_{Cu} - \Delta V/\Delta T$, where α_{Cu} is the thermopower of the copper lead.

2.5. Electrochemical Impedance Spectroscopy. Electrochemical impedance spectroscopic (EIS) measurements were carried out with an AC impedance spectroscope (Solartron 1260 FRA) in the temperature range 500−800 °C in air. A symmetrical cell SYCO|LSGM|SYCO was used for EIS measurements. For this purpose, the SYCO

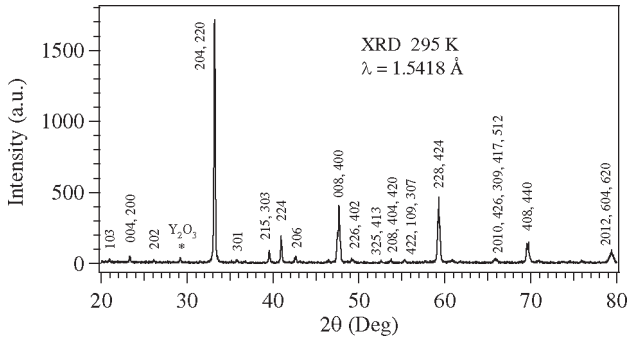

Figure 2. X-ray powder diffraction pattern of the oxygen-deficient perovskite $Sr_{0.7}Y_{0.3}CoO_{2.65-\delta}$ indexed in a tetragonal unit cell with $a \approx 7.627$ Å and $c \approx 15.31$ Å. A small amount of impurity Y_2O_3 was observed.

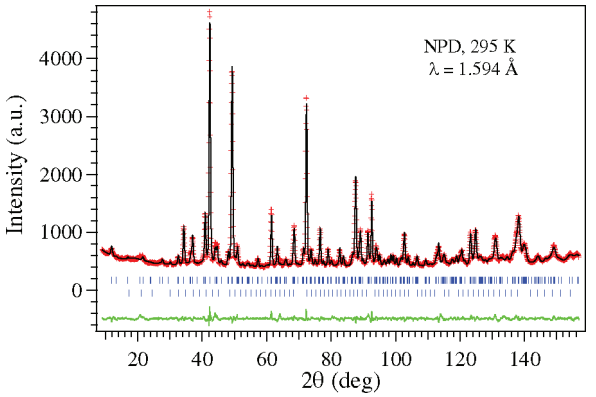

Figure 3. Observed (crosses), calculated (solid line), and difference (bottom line) neutron powder diffraction profiles of the oxygen-deficient perovskite $Sr_{0.7}Y_{0.3}CoO_{2.65-\delta}$ at room temperature. The two lines of vertical markers correspond to the allowed Bragg reflections for $Sr_{0.7}Y_{0.3}CoO_{2.65-\delta}$ (top) and Y_2O_3 (bottom).

cathode with an area of 0.25 cm^2 was screen-printed onto both sides of a dense LSGM electrolyte pellet of 600 μm thickness. After drying, the SYCO cathode was sintered at 1100 °C for 1 h in air. The frequency range from 0.01 Hz to 1 MHz was applied with a signal amplitude of 10 mV under open cell voltage.[10]

2.6. Fabrication and Testing of a Single Fuel Cell. A single electrolyte-supported test fuel cell was fabricated by using a 300-μm thick LSGM pellet as the electrolyte, SYCO as the cathode, and NiO-GDC (Gd-doped ceria) as the anode. As described elsewhere,[11] between the electrolyte and the electrodes, a thin $La_{0.4}Ce_{0.6}O_{2-\delta}$ (LDC) buffer layer was used to prevent the interdiffusion of ionic species. Details about the preparation of the LSGM electrolyte and the LDC buffer-layer material have been described elsewhere.[12] The NiO-GDC anode material was purchased from Full-Cell Materials. SYCO, LDC, and NiO-GDC powders were made into inks with a binder, V-006 (Heraeus). LDC ink was screen-printed onto both sides of the LSGM disk, followed by firing at 1300 °C in air for 1 h. NiO-GDC was subsequently screen-printed onto the LDC layer on one side and baked at 1300 °C in air for 0.5 h. Then, the SYCO was finally screen-printed onto the other side of the LSGM disk and sintered at 1100 °C in air for 1 h. The area of the working electrode is 0.24 cm^2. Pt gauze (Alfa Aesar, 52 mesh woven from 0.1 mm-diameter wire, 99.9% metal basis) with a small amount of Pt paste (Heraeus) in separate dots was used as a current collector at both the anode and cathode sides for ensuring contact. A double-layer sealing design was applied in all single-cell tests. The assembled test cell was placed in the hot zone of a vertical furnace with air directly supplied to the cathode surface and dry H_2 fuel to the anode surface at a flow rate of 30 mL/min. The performance measurements were carried out at 700, 750, and 800 °C with an EG&G potentiostat/galvanostat.[13]

3. RESULTS

3.1. Structural Characterizations. Displayed in Figure 2 is the room-temperature XRD pattern of the obtained SYCO sample, which can be indexed on the basis of a tetragonal unit cell with $a \approx 7.627$ Å and $c \approx 15.31$ Å. Thus, the cell is related to the cell parameter of a cubic perovskite a_p by $a \approx 2 \times a_p$ and $c \approx 4 \times a_p$.[6] As indicated by the asterisk (*), the obtained sample contains a small amount of Y_2O_3 impurity, probably as a result of the evaporation of Co_3O_4 at high temperatures. A similar situation has also been reported in the literature.[6] The oxygen content was determined by iodometric titration to be $Sr_{0.7}Y_{0.3}CoO_{2.63(1)}$, yielding a formal Co oxidation state of +2.96.

To extract accurate structural information for this oxygen-deficient perovskite, a room-temperature NPD pattern was refined in the tetragonal $I4/mmm$ space group (No. 139) with three kinds of Sr/Y atoms at 4e (0,0,z) and 8g (0,0.5,z), two kinds of Co atoms placed at 8h (x,x,0) and 8f (0.25,0.75,0.25), and four oxygen positions, O1 at 16n (0,y,z), O2 at 16 m (x,x,z), O3 at 8i (0,y,0), and O4 at 8j (x,0.5,0). The O4 position is partially occupied. A secondary phase Y_2O_3 defined in the space group $Ia\bar{3}$ was introduced in the refinement. The refinement converged very well with discrepancy factors of $R_p = 2.30\%$, $R_{Bragg} = 3.02\%$, and $\chi^2 = 3.88$; the goodness of fit is illustrated in Figure 3. The structural parameters and selected bond lengths and bond angles after the Rietveld refinements are given in Table 1. The unit-cell parameters, $a = 7.6258(1)$ and $c = 15.3110(4)$ Å, for our sample are in excellent agreement with those reported in the literature, such as $a = 7.6193(8)$ and $c = 15.313(2)$ Å in ref 6. From the scale factors, the Y_2O_3 impurity was estimated to be ~1.4(2) wt %. NPD also allowed us to examine the occupancy factors of the oxygen atoms. The refinement of the occupancy factors for the O1, O2, and O3 converged to values very close to 1 (Table 1), while that of the O4 position, 0.37, is a little larger than the reported 0.25 for all Co(III). On the basis of the obtained occupancy factors for oxygen positions, the chemical formula was estimated to be $Sr_{0.7}Y_{0.3}CoO_{2.66(2)}$, in accordance with the result obtained from the iodometric titration. Therefore, the valence state of the Co ions in SYCO should be mainly 3+.

The obtained Co−O bond lengths of our SYCO sample, given in Table 1, are highly consistent with those reported previously.[6] In the octahedral layers, the $Co2O_{6/2}$ octahedra exhibit a significant axial distortion with four shorter equatorial distances Co2−O1 = 1.913(2) Å and two longer axial distances Co2−O2 = 2.079(3) Å to give a $c/a \approx 1.09$. Such a tetragonal local site symmetry of Co2 would tend to stabilize an IS Co^{3+}. Corresponding to the axial elongation of the $Co2O_{6/2}$ octahedra, the $Co1O_4$ tetrahedra in the oxygen-deficient layers are compressed along the c axis with a much shorter Co1−O2 = 1.830(3) Å distance than the Co1−O3 = 1.930(4) Å lying in the ab plane. Similar to the previous report,[6] the presence of additional oxygen atoms distributed over the O4 positions within the oxygen-deficient layers result in some five-coordinated Co1 sites forming an irregular trigonal bipyramid. However, the extremely long Co1−O4 bond length of 2.147(9) Å signals a much weaker bonding strength, and the unusually high thermal factor 5.2(4) Å for the O4 atoms, Table 1, signals that it is the O4 atoms that

dx.doi.org/10.1021/cm202542q |Chem. Mater. 2011, 23, 5037–5044

Table 1. Atomic Coordinates, Isotropic Thermal Factors, and Selected Bond Length and Angles for $Sr_{0.7}Y_{0.3}CoO_{2.65-\delta}$ from Neutron Powder Diffraction Data[a] at 295 K[b]

atom	site	x	y	z	B_{iso} (Å^2)	occ.
Sr1/Y1	4e	0	0	0.8785(4)	1.79(9)	0.7/0.3[c]
Sr2/Y2	8g	0	0.5	0.8674(2)	0.95(5)	0.7/0.3[c]
Sr3/Y3	4e	0	0	0.3509(3)	0.61(8)	0.7/0.3[c]
Co1	8h	0.7481(5)	0.7481(5)	0	0.62(5)	1[c]
Co2	8f	0.25	0.75	0.25	0.62(5)	1[c]
O1	16n	0	0.2453(3)	0.2400(2)	0.54(5)	0.985(6)
O2	16m	0.2877(2)	0.2877(2)	0.1167(2)	1.67(5)	1[c]
O3	8i	0	0.7233(5)	0	1.26(8)	0.980(8)
O4	8j	0.3833(17)	0.5	0	5.2(4)	0.37(1)

bond length (Å)		bond angle (deg)	
Co1−O2 (× 2)	1.830(3)	Co2−O1−Co2	170.552(9)
Co1−O3 (× 2)	1.930(4)	Co1−O2−Co2	156.52(12)
Co1−O4 (× 1)	2.147(9)	Co1−O3−Co1	168.6(4)
Co2−O1 (× 4)	1.913(2)		
Co2−O2 (× 2)	2.079(3)		

[a] R_p = 2.30%, R_{wp} = 3.02%, R_{exp} = 1.53%, χ^2 = 3.88, and R_{Bragg} = 3.39%. [b] Space group *I4/mmm* (No. 139), a = 7.6258(1) Å, c = 15.3110(4) Å, V = 890.38(3) Å^3, Z = 16. [c] Fixed.

become mobile and disordered above 320 °C. The exolution and diffusion of these oxygen atoms within the oxygen-deficient layers plays an important role for both the electronic transport (see section 3.3) and the O^{2-}-ion conduction at elevated temperatures, which are essential ingredients for high-performance MIEC cathode materials of IT-SOFCs.

To reveal the thermal evolution of the loosely bonded O4 atoms within the oxygen-deficient layers, we measured the TGA curves of the SYCO sample upon thermal cycling between 30 and 900 °C in air with a heating/cooling rate of 2 °C/min. The TGA data are displayed in Figure 4. Up to 800 °C, the highest temperature for electrochemical performance measurements in the present study, the SYCO sample experiences a slight weight loss of 0.25%, corresponding to only ∼1.1% of total oxygen content or 25% of the O4 atoms, which means that most of the weakly bounded O4 atoms are still present up to 800 °C. These data are consistent with the TGA results of Istomin et al.,[6] where a complete removal of O4 atoms was only realized at 1000 °C in helium. As shown in Figure 4, the SYCO sample starts to lose weight immediately upon heating from room temperature; the oxygen exolution increases at temperatures above 325 and 800 °C. Because the TGA curve during cooling completely restored the one upon heating, the weight change between 30 and 320 °C is not likely due to the absorption of moisture, but rather it is likely due to the exolution of weakly bonded O4 atoms in the SYCO samples.

High-temperature NPD patterns collected up to 800 °C further confirmed that the crystal structure remains unchanged. Because of the strong reflections from the steel container, only the unit-cell parameters were refined in the first run from the HT-NPD data. As shown in Figure 5, the lattice parameters expand with increasing temperature. On the basis of the unit-cell volume at 25 and 800 °C, the linear thermal expansion coefficient (TEC) can be estimated as 19.6 × 10^{-6} K^{-1}, which is comparable to other cobalt-containing perovskites.[2,3] With all other parameters fixed in the second refinements, the occupancy factors of the O4 atom have been tentatively opened and the obtained ∼30%

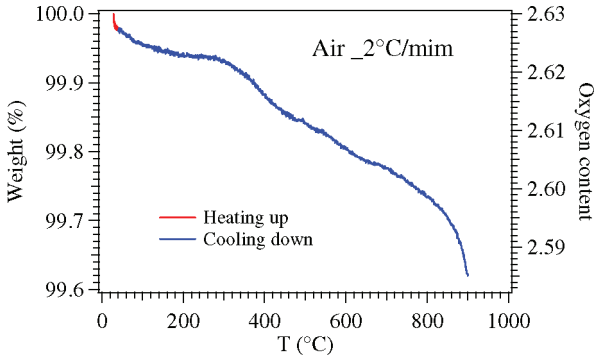

Figure 4. TGA curves and the corresponding oxygen content of oxygen-deficient perovskite $Sr_{0.7}Y_{0.3}CoO_{2.65-\delta}$ measured upon heating up and cooling down between room temperature and 900 °C in air.

decrease in this temperature interval is consistent with the above TGA results.

3.2. X-ray Absorption Spectroscopy. Figure 6 shows the O1s spectrum of SYCO, together with that of $EuCoO_3$ as a LS Co^{3+} reference and Sr_2CoO_3Cl as a high spin Co^{3+} reference, taken from Hu et al.[14] The reference spectra demonstrate the high sensitivity of the O−K edge to the spin state. The pre-edge peak of SYCO lies 1 eV lower in energy than that of the LS Co^{3+} $EuCoO_3$ and is close to that of the Co^{3+} in Sr_2CoO_3Cl, indicating that the Co^{3+} in SYCO can definitely not be LS. Yet, whether all the Co^{3+} ions are in the HS or IS state is not clear at the moment and is, in fact, also not relevant for the present study.

Figure 7 shows the experimental Co−$L_{2,3}$ XAS spectra of SYCO (black line), together with $EuCoO_3$ (blue line) and Sr_2CoO_3Cl (magenta line) for comparison.[14] One can see that the overall spectral shape and L_3/L_2 intensity ratio of SYCO are very different from those of a LS Co^{3+} $EuCoO_3$ and rather similar to those of the Co^{3+} in Sr_2CoO_3Cl. It is known that the L_3/L_2 intensity ratio is very sensitive to the spin state of the ion;[15−18] so, this demonstrates once again that the Co^{3+} ions in SYCO cannot

dx.doi.org/10.1021/cm202542q |*Chem. Mater.* 2011, 23, 5037–5044

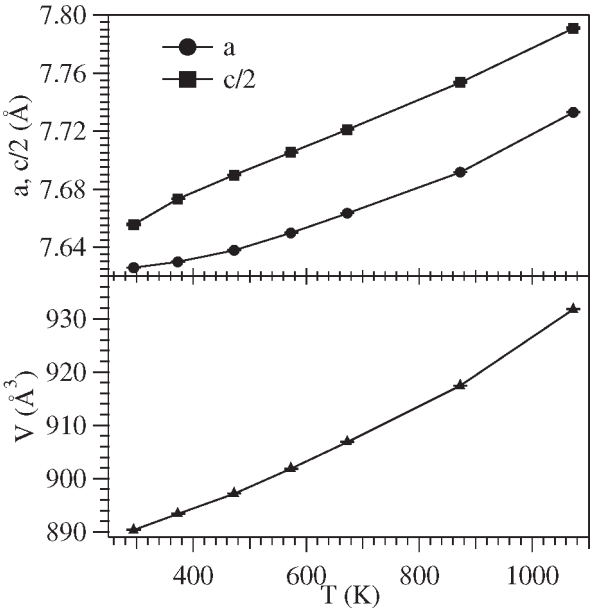

Figure 5. Thermal variation of the unit-cell parameters and volume of $Sr_{0.7}Y_{0.3}CoO_{2.65-\delta}$ from *in situ* NPD data.

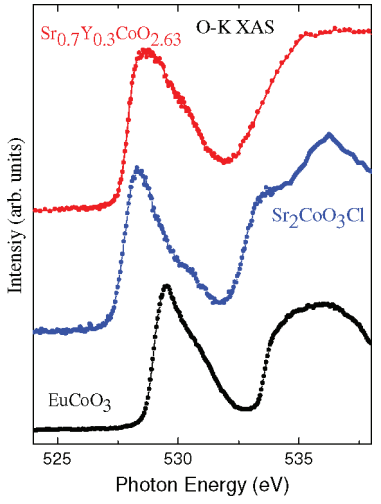

Figure 6. O−K-edge X-ray absorption spectroscopy of the oxygen-deficient perovskite $Sr_{0.7}Y_{0.3}CoO_{2.65-\delta}$, together with $EuCoO_3$ (black line) and Sr_2CoO_3Cl (blue line) for comparison.

be LS. Whether they are HS or LS will need further investigations because the different local environments of the Co^{3+} ions may affect further details of the line shape. As far as the Co^{2+} ions are concerned, it is known from previous studies that they are in the very stable HS state.[14,19]

3.3. Electrical Transport Properties. Figure 8a shows the temperature dependence of the electrical resistivity $\rho(T)$ in a logarithmic scale (left) and the conductivity $\sigma(T) = 1/\rho(T)$ in a linear scale (right) measured on a sintered SYCO pellet over a wide temperature range from 100 to 1073 K. The SYCO sample shows a semiconducting behavior at low temperature; the resistance becomes too large for us to measure below 100 K. With increasing temperature, $\rho(T)$ first decreases sharply by six orders from 10^4 to 10^{-2} Ω cm up to 400 K, then it exhibits a much weaker temperature dependence and even becomes

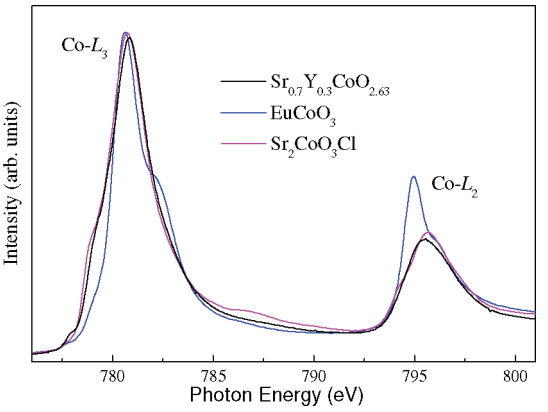

Figure 7. Experimental Co−$L_{2,3}$ XAS spectra of $Sr_{0.7}Y_{0.3}CoO_{2.65-\delta}$ (black line), together with $EuCoO_3$ (blue line) and Sr_2CoO_3Cl (magenta line).

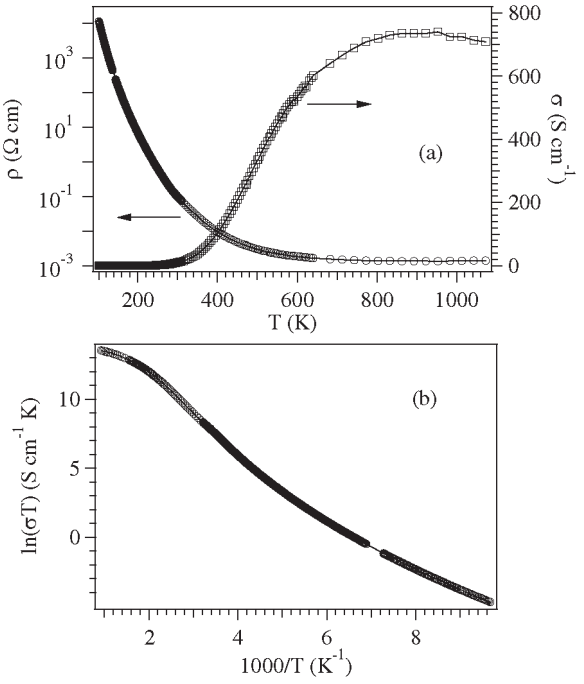

Figure 8. (a) Temperature dependence of the electrical resistivity $\rho(T)$ in a semilog scale (left) and the conductivity $\sigma(T)$ in a linear scale (right). (b) Arrhenius plot, $\ln(\sigma T)$ vs 1000/T, for the oxygen-deficient perovskite $Sr_{0.7}Y_{0.3}CoO_{2.65-\delta}$ measured in air in a wide temperature range 100−1073 K.

metallic above 900 K; $\sigma(T)$ exceeds 700 S cm^{-1} for T > 500 °C with a broad maximum of 735 S cm^{-1} near 650 °C. Such a high electrical conductivity satisfies the general requirement for the cathode materials of a SOFC, that is, > 100 S cm^{-1}. To understand the mechanism for the electrical conduction in SYCO, we have replotted the $\sigma(T)$ data in the form of $\ln(\sigma T)$ vs $1000/T$ in Figure 8b. As can be seen, the Arrhenius plot does not produce a straight line in the whole temperature range, indicating a variation of the conduction mechanism with temperature. Similar nonlinear behavior of conductivity has also been reported by Istomin, et al.[20] and was attributed to the gradual change of oxygen concentration rather than of O4

dx.doi.org/10.1021/cm202542q |*Chem. Mater.* 2011, 23, 5037–5044

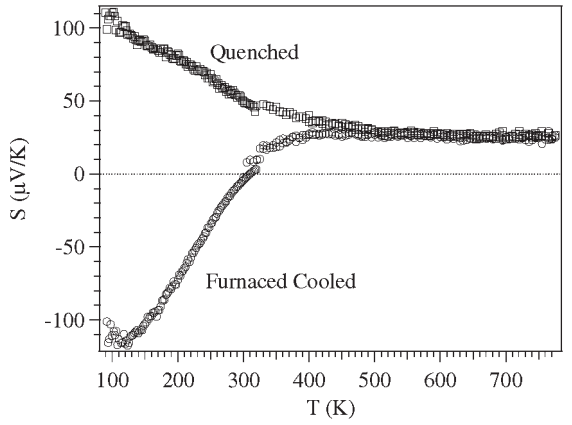

Figure 9. Temperature dependence of the thermopower $S(T)$ of the oxygen-deficient perovskite $Sr_{0.7}Y_{0.3}CoO_{2.65-\delta}$ prepared via furnace-cooling and quenching to room temperature.

disorder with increasing temperature. As shown by the solid line in Figure 8b, linear fitting to the Arrhenius plot below 200 K yields an activation energy of ~128 meV.

To reveal the nature of the charge carries, especially above 400 K, we resorted to measurements of the thermopower $S(T)$ of the SYCO sample over a wide temperature range from 100 to 773 K. Figure 9 presents the $S(T)$ data for the two SYCO samples, the furnace-cooled one and the quenched one. In a previous study,[9] $S(T)$ data for various SYCO samples treated under different conditions were measured below room temperature, and it was noted that the $S(T)$ of a furnace-cooled SYCO sample undergoes a sign crossover near RT and exhibits completely different behavior compared to the quenched sample. The same result is also shown in Figure 9. More interestingly, the $S(T)$ of these two SYCO samples approach the same constant value of ca. +25 μV/K above 450 K, indicating p-type charge carriers in the high-T conductive phase. Such a variation of $S(T)$ is consistent with the weak temperature dependence and highly conductive behavior in $\rho(T)$. Although the iodometric titration showed that the quenched sample is slightly oxygen deficient relative to the furnace-cooled one at room-temperature, the $S(T)$ behavior clearly indicates that the transport properties of their final states are identical and the variation of the $S(T)$ data is more likely to be correlated with the order−disorder transition of the oxygen vacancies within the oxygen-deficient layers than with the oxygen concentration; high-temperature synchrotron XRD measurements[8] have shown that oxygen vacancies undergo an order−disorder transition at $T_s \sim 550$ K for $Sr_{0.67}Y_{0.33}CoO_{3-\delta}$. The oxygen vacancies remain disordered in the quenched sample. Previous $S(T)$ for oxygen-deficient perovskites $Sr_{1-x}R_xCoO_{3-\delta}$ (R = rare earth) have been made only below room temperature. As a follow-up to the previous study on the thermoelectric properties,[9] such a small value of $S(T)$ at high temperatures shows that SYCO is not suitable for high-temperature thermoelectric applications. However, the high electronic conductivity and the large amount of disordered oxygen vacancies as well as the presence of loosely bound O4 atoms motivated us to evaluate the electrochemical performance of SYCO as a potential cathode material for IT-SOFCs.

3.4. Electrochemical Performance. The electrode performance was first evaluated by electrochemical impedance spectroscopy (EIS) on a symmetrical cell SYCO|LSGM|SYCO over the temperature range 500−800 °C in air. A SYCO cathode with an area of 0.25 cm^2 was screen-printed onto both sides of a dense LSGM electrolyte pellet of 600 μm thickness. Figure 10a displays typical impedance spectra obtained at 700, 750, and 800 °C in air. The impedance response for oxygen reduction on SYCO is characterized as a depressed arc. The high-frequency intercept of the electrode impedance on the real axis is the total resistance of the electrolyte. The difference between the low-frequency and the high-frequency intercepts on the real axis corresponds to the area specific resistance (ASR) of the two

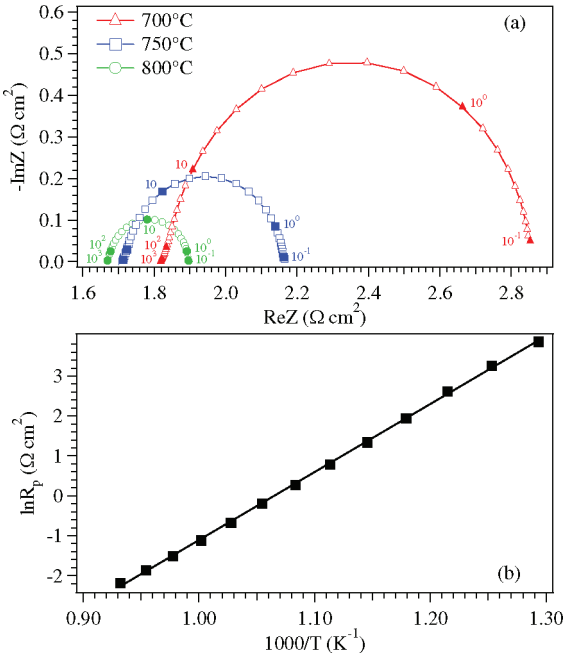

Figure 10. (a) Typical impedance spectra of the oxygen-deficient perovskite $Sr_{0.7}Y_{0.3}CoO_{2.65-\delta}$ cathode on an LSGM electrolyte measured at 700−800 °C in air and (b) the Arrhenius plot of the ASR for SYCO cathode.

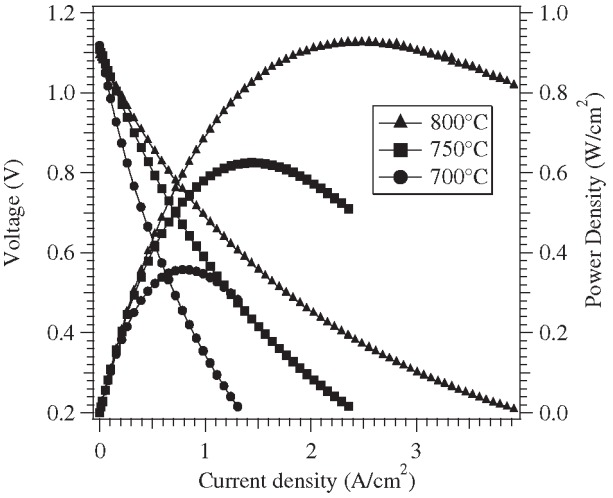

Figure 11. Cell voltage (left) and power density (right) as a function of the current density for the SYCO|LSGM|NiO-GDC test cell at different temperatures.

dx.doi.org/10.1021/cm202542q |*Chem. Mater.* 2011, 23, 5037–5044

interfaces. The ASR is the overall resistance related to the oxygen reduction, oxygen surface/bulk diffusion, and the gas-phase oxygen diffusion. As can be seen, the ASR value reduces significantly with increasing temperature and reaches 0.11 Ω cm^2 at 800 °C, which indicates that SYCO has high electrocatalytic activity for the ORR at intermediate temperatures. The corresponding activation energy calculated from the slope of Figure 10b is 1.46 eV.

The performance of the SYCO cathode was then tested in a single cell. Figure 11 depicts the cell voltage and power density as a function of current density for the single fuel cell NiO-GDC|LSGM|SYCO operating at different temperatures with dry hydrogen as fuel and ambient air as oxidant. The maximum power densities P_{max} reach 359, 626, and 927 mW/cm^2 at 700, 750, and 800 °C, respectively, nearly double the practical requirements of 500 mW/cm^2 at 800 °C for a single cell. Such an excellent cell performance demonstrates that SYCO is a promising cathode material for IT-SOFCs.

4. DISCUSSION

Like all the best MIEC cathodes known for a SOFC, SYCO is a good MIEC containing Co(III) cations in an oxygen-deficient perovskite structure at operating temperature T_{op} > 600 °C. However, the change from n-type polaronic conduction to p-type itinerant-electron conduction on the disordering the O4 atoms in the $Co1O_{1.15-\delta}$ planes despite an accompanying small O^{2-} ion loss is remarkable. The n-type polaronic conduction at room temperature is consistent with a small concentration of Co(II) in accordance with the oxygen stoichiometry $Sr_{0.7}Y_{0.3}CoO_{2.65-\delta}$ (δ = 0.02).

To understand the electronic transition to p-type itinerant-electron behavior, we consider the spin-state transitions that occur on an octahedral-site Co(III) ion in an oxoperovskite and the relative site-preference energy of the Co(II) versus Co(III) for tetrahedral or trigonal bipyramidal sites. In $LaCoO_3$, at low temperature, the bulk Co(III) are in their low-spin state Co(III): t^6e^0, but the surface Co(III) are in the higher spin state Co(III): t^5e^1 or t^4e^2. With increasing temperature, the bulk low-spin Co(III) ions transform progressively to a higher spin state. Above about 600 °C, the σ-bonding 3d electrons on the bulk Co(III) change from localized to itinerant-electron σ^* orbitals. We note that the spinel Co_3O_4 contains high-spin Co(II):e^4t^3 on the tetrahedral site and low-spin Co(III) on the octahedral sites. Therefore, we conclude that the Co(II) of SYCO have a preference for the Co1 of the $Co1O_{1.15-\delta}$ planes. The ordering of the O4 atoms apparently traps the minority-spin Co1 e^2 electrons on Co(II) in a local site deformation that renders them polaronic. A transition to itinerant minority-spin electrons in the $Co1O_{1.15-\delta}$ planes with disordering of the O4 atoms in those planes would result in a minority-spin band more than half-filled, even with the loss of oxygen, to give p-type itinerant electron behavior.

We turn, finally, to the activity of SYCO for the ORR. The higher room temperature activity in alkaline solution for the ORR on oxoperovskites with surface cations containing an e^1 configuration has been noted and rationalized as resulting from the displacement of a surface OH^- species by an adsorbed $(O_2)^-$ ion as the rate-determining step.[21] At high temperature, the bound water is lost, but surface intermediate-spin Co(III) can accommodate to the lower oxygen coordination at the surface without the need for a surface reconstruction because the higher spin Co(III) is stable in 4-, 5-, and 6-fold coordination. Indeed, it is this ability that is responsible for the surface ferromagnetism of low-temperature $LaCoO_3$. An adsorbed O_2 molecule is able to transform, in a step not involving surface reconstruction, both a 4- and a 5-coordinate surface Co(III):t^5e^1 or t^4e^2 site to a 6-coordinated Co(IV) site by becoming $(O_2)^-$; the initial removal of Li from layered $LiCoO_2$ introduces high-spin Co-(IV):t^3e^2, while subsequent Li removal creates low-spin Co-(IV):$\pi^{*5}\sigma^{*0}$. Because SYCO is a MIEC, the adsorbed $(O_2)^-$ can be rapidly reduced to $2O^{2-}$ that are transported to the O^{2-}-ion electrolyte.

5. CONCLUSION

The oxygen-deficient perovskite $Sr_{0.7}Y_{0.3}CoO_{2.65-\delta}$ (SYCO) contains alternate (001) planes of $Co2O_{6/2}$ octahedra and $Co1O_{1.15-\delta}$ planes containing 4- and 5- coordinated cobalt; the room-temperature oxygen stoichiometry $\delta \approx 0.02$ signals mostly Co(III) with $2\delta \approx 0.04$ Co(II)/formula unit. The coordinations of the Co1 sites are favorable for occupancy by high-spin or intermediate-spin Co(III) and high-spin Co(II). A small oxygen loss with increasing temperature to 800 °C signals some increase in the Co(II) concentration, but full oxygen loss of O4 from the $Co1O_{1.15-\delta}$ planes to $Co1O_1$ only occurs at 1000 °C in helium where the brownmillerite structure is realized. Below 300 °C, the O4 atoms of the $Co1O_{1.15-\delta}$ planes are ordered and the Co(II) give n-type polaronic conduction. Above 600 °C, the O4 are disordered and mobile, while the minority-spin electrons in the $Co1O_{1.15-\delta}$ planes become itinerant to give a p-type itinerant-hole behavior. Above 600 °C, SYCO is a MIEC exhibiting good activity for the ORR, which makes it a competitive cathode material for an IT-SOFC.

AUTHOR INFORMATION

Corresponding Author

*E-mail: jgoodenough@mail.utexas.edu.

ACKNOWLEDGMENT

Y.L. thanks Dr. Jianshi Zhou for helping with some measurements and for useful discussions. This work was supported by Robert A. Welch Foundation, Houston, TX (Grant Nos. F-1066 and F-1254). J.A.A. thanks the financial support of the Spanish Ministry of Education to the project MAT2010-16404. We are grateful to the Institut Laue-Langevin (ILL) for making all the facilities available.

REFERENCES

(1) Stevenson, J. W.; Armstrong, T. R.; Carneim, R. D.; Pederson, L. R.; Weber, W. J. *J. Electrochem. Soc.* **1996**, *143*, 2722.

(2) Shao, Z. P.; Haile, S. M. *Nature* **2004**, *431*, 170.

(3) Pena-Martinez, J.; Marrero-Lopez, D.; Ruiz-Morales, J. C.; Buergler, B. E.; Nunez, P.; Gauckler, L. J. *Solid State Ionics* **2006**, *177*, 2143.

(4) Tarancon, A.; Skinner, S. J.; Chater, R. J.; Hernandez-Ramirez, F.; Kilner, J. A. *J. Mater. Chem.* **2007**, *17*, 3175.

(5) Kim, J.-H.; Manthiram, A. *J. Electrochem. Soc.* **2008**, *155*, B385.

(6) Istomin, S. Ya.; Grins, J.; Svensson, G.; Drozhzhin, O. A.; Kozhevnikov, V. L.; Antipov, E. V.; Attfield, J. P. *Chem. Mater.* **2003**, *15*, 4012.

(7) Withers, R. L.; James, M.; Goossens, D. J. *J. Solid State Chem.* **2003**, *174*, 198.

(8) Khalyavin, D. D.; Chapon, L. C.; Suard, E.; Parker, J. E.; Thompson, S. P.; Yaremchenko, A. A.; Kharton, V. V. *Phys. Rev. B* **2011**, *83*, 140403(R).
(9) Takami, T.; Cheng, J. G. *J. Appl. Phys.* **2011**, *50*, 013002.
(10) Kim, Y. N.; Kim, J.-H.; Manthiram, A. *J. Power Sources* **2010**, *195*, 6411.
(11) Wan, J. H.; Yan, J. Q.; Goodenough, J. B. *J. Electrochem. Soc.* **2005**, *152*, A1511.
(12) Huang, Y. H.; Dass, R. I.; Xing, Z. L.; Goodenough, J. B. *Science* **2006**, *312*, 254.
(13) Huang, Y. H.; Dass, R. I.; Denyszyn, J. C.; Goodenough, J. B. *J. Electrochem. Soc.* **2006**, *153*, A1266.
(14) Hu, Z.; Wu, H.; Haverkort, M. W.; Hsieh, H. H.; Lin, H.-J.; Lorenz, T.; Baier, J.; Reichl, A.; Bonn, I.; Felser, C.; Tanaka, A.; Chen, C. T.; Tjeng, L. H. *Phys. Rev. Lett.* **2004**, *92*, 207402.
(15) van der Laan, G.; Thole, B. T.; Sawatzky, G. A.; Verdaguer, M. *Phys. Rev. B* **1988**, *37*, 6587.
(16) Thole, B. T.; van der Laan, G. *Phys. Rev. B* **1988**, *38*, 3158.
(17) dit Moulin, C. C.; Rudolf, P.; Flank, A.-M.; Chen, C. T. *J. Phys. Chem.* **1992**, *96*, 6196.
(18) Pen, H. F.; Tjeng, L. H.; Pellegrin, E.; de Groot, F. M. F.; Sawatzky, G. A.; van Veenendaal, M. A.; Chen, C. T. *Phys. Rev. B* **1997**, *55*, 15500.
(19) Hollmann, N.; Hu, Z.; Valldor, M.; Maignan, A.; Tanaka, A.; Hsieh, H. H.; Lin, H.-J.; Chen, C. T.; Tjeng, L. H. *Phys. Rev. B* **2009**, *80*, 085111.
(20) Istomin, S. Ya.; Drozhzhin, O. A.; Napolsky, Ph. S.; Putilin, S. N.; Gippius, A. A.; Antipov, E. V. *Solid State Ionics* **2008**, *179*, 1054.
(21) Suntivich, J.; Gasteiger, H. A.; Yabuuchi, N.; Nakanishi, H.; Goodenough, J. B.; Yang, S. H. *Nature Chem.* **2011**, *3*, 546.